ACS NANO
Cite This: ACS Nano 2017, 11, 9989-9996
www.acsnano.org

ARTICLE

Chemical and Electronic Repair Mechanism of Defects in MoS_2 Monolayers

Anja Förster,[†,‡,¶] Sibylle Gemming,[‡,§,∥] Gotthard Seifert,[‡,¶,⊥] and David Tománek*[,†]

[†]Physics and Astronomy Department, Michigan State University, East Lansing, Michigan 48824, United States
[‡]Center for Advancing Electronics Dresden (cfaed), 01062 Dresden, Germany
[¶]Theoretical Chemistry, Technische Universität Dresden, 01062 Dresden, Germany
[§]Helmholtz-Zentrum Dresden-Rossendorf, Institute of Ion Beam Physics and Materials Research, Bautzner Landstrasse 400, 01328 Dresden, Germany
[∥]Institute of Physics, Technische Universität Chemnitz, 09107 Chemnitz, Germany
[⊥]National University of Science and Technology, MISIS, 119049 Moscow, Russia

ABSTRACT: **Using *ab initio* density functional theory calculations, we characterize changes in the electronic structure of MoS_2 monolayers introduced by missing or additional adsorbed sulfur atoms. We furthermore identify the chemical and electronic function of substances that have been reported to reduce the adverse effect of sulfur vacancies in quenching photoluminescence and reducing electronic conductance. We find that thiol-group-containing molecules adsorbed at vacancy sites may reinsert missing sulfur atoms. In the presence of additional adsorbed sulfur atoms, thiols may form disulfides on the MoS_2 surface to mitigate the adverse effect of defects.**

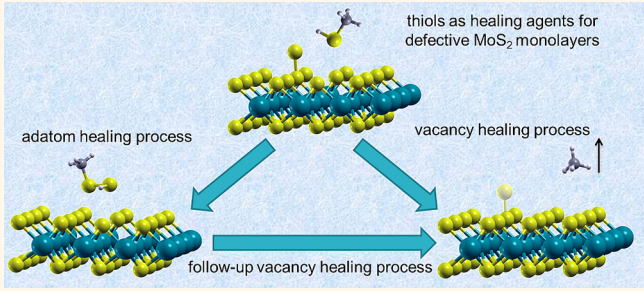

KEYWORDS: *transition metal dichalcogenides, 2D materials, ab initio calculations, electronic structure, defects*

There is growing interest in two-dimensional (2D) transition metal dichalcogenide (TMD) semiconductors, both for fundamental reasons and as potential components in flexible, low-power electronic circuitry and for sensor applications.[1−3] Molybdenum disulfide, MoS_2, is a prominent representative of this class of TMDs. A free-standing, perfect 2D MoS_2 monolayer possesses a direct band gap of 1.88 eV at the *K*-point in the Brillouin zone.[4,5] Most commonly used production methods for MoS_2 monolayers are chemical vapor deposition (CVD) and mechanical exfoliation of the layered bulk material,[6−8] as well as sputter growth atomic layer deposition[9] (ALD) of the precursor MoO_3 and subsequent conversion to the disulfide under reducing conditions and at high temperatures.[10,11] A direct ALD process using H_2S and $MoCl_5$[12] or $Mo(CO)_6$[13] is another possibility to obtain MoS_2 monolayers. The CVD technique is probably best suited for mass production, but the synthesized MoS_2 layers lack atomic perfection. The most common defects in these layers are sulfur and molybdenum vacancies, as well as additional adsorbed sulfur atoms.[14−19] Eliminating or at least reducing the adverse effect of such defects is imperative to improve the optoelectronic and transport properties of TMDs.

In search of ways to mitigate the adverse effect of defects, different methods have been suggested, including exposure of MoS_2 to superacids[20] or thiols.[21,22] In the related $MoSe_2$ system, Se vacancies could be filled by S atoms from an adjacent MoS_2 layer.[23] In the present study, we focus on the reactions of thiols with defective MoS_2 monolayers.

First, we characterize changes in the electronic structure of MoS_2 monolayers introduced by missing or additional adsorbed sulfur atoms using *ab initio* density functional theory (DFT) calculations. We provide microscopic information about the chemical and electronic function of thiols as a theoretical background for the understanding of the successful use of thiols, which have been reported to reduce the adverse effect of sulfur vacancies in quenching photoluminescence and to improve the electronic conductance of defective MoS_2. We found that adsorbed thiols may reinsert missing sulfur atoms at vacancy sites. We also found that in the presence of sulfur adatoms thiols will form disulfides on the MoS_2 surface, which mitigates the adverse effect of defects.

In Figure 1 we display the structure of a defective MoS_2 monolayer with a sulfur monovacancy (V) and an additional sulfur adatom (A), since these defects are known to significantly affect the electronic properties of MoS_2.[24] The formation energy of the sulfur vacancy is 2.71 eV, and that of

Received: June 14, 2017
Accepted: September 15, 2017
Published: September 15, 2017

DOI: 10.1021/acsnano.7b04162
ACS Nano 2017, 11, 9989−9996

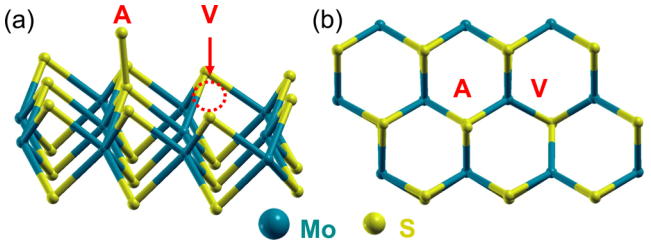

Figure 1. (a) Perspective and (b) top view of the optimized geometry of an MoS_2 monolayer containing a sulfur monovacancy (V) and a sulfur adatom (A).

the sulfur adatom is 1.07 eV. Consequently, the recombination energy of a sulfur vacancy and a sulfur adatom is −1.89 eV. In spite of the large energy gain, no spontaneous healing will occur in a system with both defect types present due to the high activation barrier of ≈1.5 eV for this reaction. The listed defect formation energies are in agreement with a study reporting the effect of various defect types on the electronic structure of MoS_2[25] and also with a study of vacancy defects.[26]

Defects affect drastically the electronic structure in the vicinity of the Fermi level. Setting apart the inadequacy of DFT-PBE (Perdew−Burke−Ernzerhof) calculations for quantitative predictions of band gaps, we should note that in our computational approach with (large) supercells and periodic boundary conditions also defects form a periodic array. In spite of their large separation, defect states evolve into narrow bands that may affect the band structure of a pristine MoS_2 monolayer. The effect of a sulfur monovacancy, as well as that of a sulfur adatom, on the density of states (DOS) of a MoS_2 monolayer around the band gap region is shown in Figure 2.

As seen in Figure 2c, sulfur monovacancies introduce defect states within the band gap, and their superlattice shifts the DOS down by 0.16 eV with respect to the pristine lattice. The defect states are localized around the vacancy as seen in Figure 2a. The effect of a superlattice of sulfur adatoms, addressed in Figure 2b and d, is to reduce the DFT band gap from 1.88 to 1.72 eV, in agreement with published results.[24,25]

Defect sites play an important role as catalytically active centers[13] and as sites for functionalization reactions of 2D MoS_2.[27] Sulfur vacancies in particular are considered to be important nucleation sites for a functionalization with thiol molecules R−SH. The likely possibility of an adsorbed thiol group transferring a sulfur atom to the vacancy and thus repairing the defect is particularly appealing. In this case, the detached hydrogen atom may reconnect with the remaining R to form R−H and fill the vacancy site of MoS_2 with sulfur, as

$$\mathrm{R{-}SH} + \mathrm{MoS_2^V} \rightarrow \mathrm{R{-}H} + \mathrm{MoS_2} \quad (1)$$

where MoS_2^V denotes the MoS_2 layer with a sulfur vacancy.

An alternative reaction has been proposed to benefit from the STM tip current in an STM study.[22] In the first step of reaction 2, similar to reaction 1, a hydrogen atom is removed from the thiol as its sulfur atom fills the previous vacancy, determining the reaction barrier for both reactions 1 and 2a. The removed hydrogen atom will then form H_2 and desorb from the MoS_2 surface. The remaining R is still bound to the sulfur atom, adsorbed at the sulfur vacancy site. The final assumption of the proposed mechanism[22] is that the R-groups are removed with the support of the STM tip, as represented in reaction 2b.

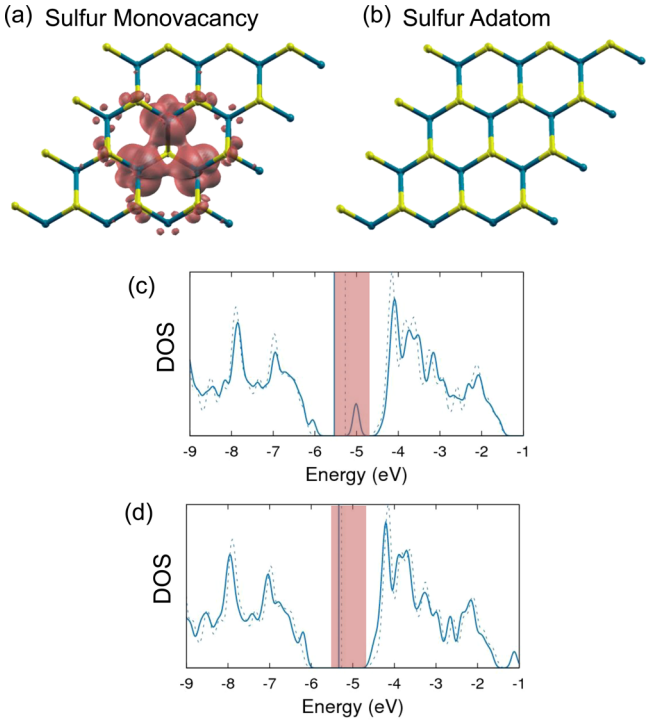

Figure 2. Ball-and-stick models of (a) a sulfur vacancy defect and (b) a sulfur adatom defect in a MoS_2 monolayer. Density of states (DOS) of MoS_2 with (c) a vacancy and (d) an adatom defect. The DOS and the position of the Fermi level are shown by solid blue lines in defective lattices and by dotted blue lines in the corresponding pristine lattices in (c) and (d). The DOS has been convoluted by a Gaussian with a full-width at half-maximum of 0.1 eV. The energy range of interest in the gap of the pristine lattice is highlighted in red. The local density of states (LDOS), representing the charge density associated with this highlighted energy range, is represented by an isosurface and superposed to the structure of a vacancy defect in (a) and an adatom defect in (b). The isosurface value in the LDOS plots is 0.003 e/bohr^3.

$$\mathrm{R{-}SH} + \mathrm{MoS_2^V} \rightarrow \frac{1}{2}\mathrm{H_2} + \mathrm{R{-}S{-}MoS_2^V} \quad (2a)$$

$$\mathrm{R{-}S{-}MoS_2^V} \xrightarrow{\mathrm{STM}} \mathrm{R\bullet} + \mathrm{MoS_2} \quad (2b)$$

There is evidence in the literature supporting both reaction 1 (refs 21, 28, 29) and reaction 2 (ref 22).

The authors of ref 30 propose yet another reaction (3a). Instead of the thiol molecules repairing the sulfur vacancy, they form an adsorbed R−SS−R disulfide at the surface of MoS_2 while releasing a hydrogen molecule. We also considered the possibility that instead of desorbing, the hydrogen molecule will fill the vacancy defect as described in reaction 3b,

$$2\mathrm{R{-}SH} + \mathrm{MoS_2} \rightarrow \mathrm{R{-}SS{-}R} + \mathrm{H_2} + \mathrm{MoS_2} \quad (3a)$$

$$2\mathrm{R{-}SH} + \mathrm{MoS_2^V} \rightarrow \mathrm{R{-}SS{-}R} + \mathrm{H_2{-}MoS_2^V} \quad (3b)$$

Based on a previous study[31] and the observation of H_2S as well as $H_3C{=}CH_3$ during the reaction of C_2H_5SH with bulk MoS_2 in ref 28, we also considered a sulfur atom adsorbed on the MoS_2 surface, identified as MoS_2^A, as the driving force for the observed disulfide formation.

In this case, the reaction to form the disulfide R−SS−R is divided into the following two steps. In reaction 4a, one thiol reacts with the adatom to R−S−S−H and, in the follow-up

DOI: 10.1021/acsnano.7b04162
ACS Nano 2017, 11, 9989−9996

reaction 4b with a second thiol, to R−S−S−R. An alternative reaction with a sulfur vacancy following reaction 4a is also possible. Similar to reaction 1, the SH-group of R−S−S−H can heal the vacancy defect, leading to the reduction of R−S−S−H to the thiol R−S−H in reaction 4c,

$$R{-}SH + MoS_2^A \rightarrow R{-}SS{-}H + MoS_2 \quad (4a)$$

$$R{-}SH + R{-}S{-}S{-}H \rightarrow H_2S + R{-}SS{-}R \quad (4b)$$

$$R{-}SS{-}H + MoS_2^V \rightarrow R{-}SH + MoS_2 \quad (4c)$$

To better understand the above reaction mechanisms 1−4, we performed DFT calculations to compare the energy associated with the pathways of these reactions. For the sake of easy understanding, we consider the small methanethiol molecule CH_3SH as a representative of thiols.

We limit our study of vacancy repair processes to reactions with MoS_2 monolayers that contain one sulfur monovacancy per unit cell. We analyze which reactions with thiols are favorable to repair vacancy and adatom defects. Our results also unveil the likely cause of apparent contradictions in the interpretation of experimental results obtained by different researchers.

RESULTS AND DISCUSSION

Vacancy Repair. The majority of published results indicate that thiol molecules interacting with sulfur-deficient MoS_2 may fill in sulfur atoms at the vacancy defect sites. Reaction pathways for the two vacancy-healing reactions 1 and 2a, which have been proposed in the literature,[22,28,29] are sketched in Figure 3. We note that reaction 1 has been studied in greater detail for a different thiol[21] and agrees with our findings for the model compound $H_3C{-}SH$.

We find that reactions 1 and 2a are both exothermic and require crossing only a low activation barrier of 0.22 eV, since they share the same transition state shown in Figure 3. The larger energy gain $E_R = -3.09$ eV in reaction 1 in comparison to −0.90 eV in reaction 2a suggests that the former reaction is thermodynamically preferred.

Figure 4a shows the DOS and partial densities of states (PDOS), projected on individual atoms, of the product of reaction 1. Figure 4b provides the corresponding information for reaction 2a, and Figure 4c provides a detailed view of the PDOS for the CH_3-group and the connected sulfur atom. In both cases, the defect states associated with sulfur monovacancies have been removed. In the final state of reaction 1 the DOS is completely restored to the undamaged state of the semiconductor. For reaction 2a, on the other hand, the Fermi level is shifted to the lower edge of the conduction band due to the CH_3-group. Therefore, only the preferred repair reaction 1 leads to both an electronic and a chemical repair of MoS_2.

Disulfide Formation. A different reaction scenario (3a) has been proposed in ref 30, suggesting that disulfides are formed when thiols interact with MoS_2. We investigated the MoS_2 surface both in its pristine state and in the presence of sulfur vacancies to clarify the differences in the catalytic potential for disulfide formation. Figure 5 illustrates reaction 3a on pristine MoS_2 and reaction 3b on a sulfur-deficient MoS_2 substrate. The schematic reaction profile indicates that both reactions involve significant activation barriers. As seen in Figure 5, reaction 3a is endothermic with a reaction energy of $E_R = 0.39$ eV and involves a high activation barrier of 2.91 eV. Reaction 3b near a sulfur monovacancy is only slightly endothermic, with a

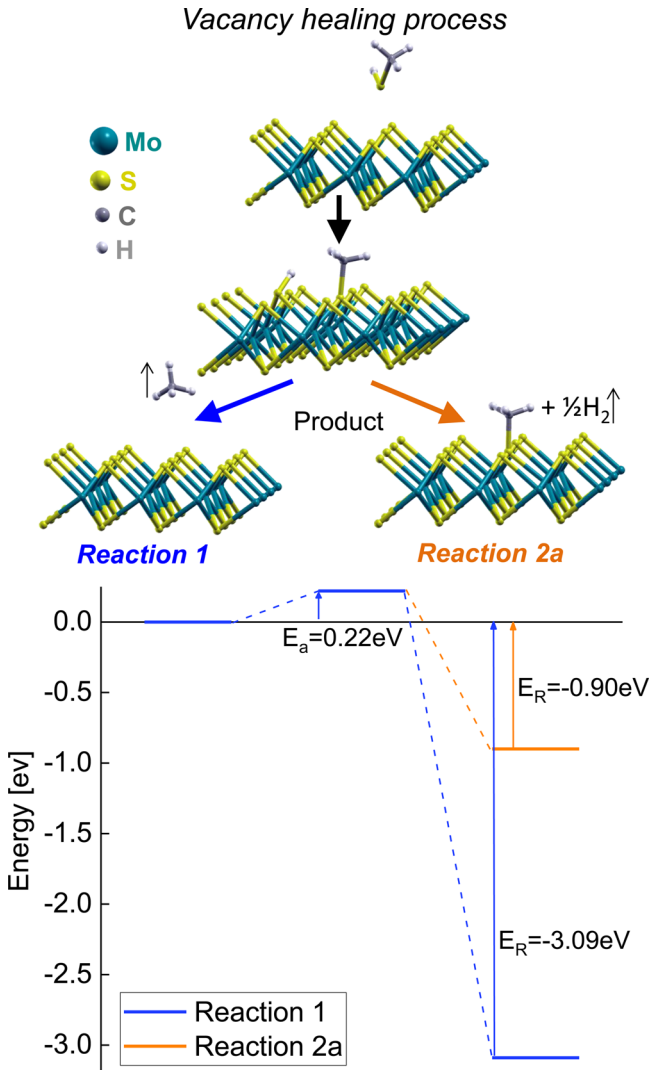

Figure 3. Reaction scheme for the sulfur vacancy healing process caused by exposure of MoS_2 with vacancies to CH_3SH. E_R denotes the reaction energy and E_a the activation barrier. The same initial state can lead to two different final states *via* the same transition state. The favorable reaction 1, shown in dark blue, leads to a free CH_4 molecule. The energetics of reaction 2a is displayed in light orange.

reaction energy $E_R = 0.02$ eV, and involves a somewhat lower activation barrier of 2.13 eV. Thus, reaction 3b is energetically more favorable than reaction 3a.

The near-neutral reaction energy of reaction 3b can be explained by the Kubas interaction of transition metal η^2-H_2 complexes.[32,33] It means that the excess H_2 molecule in the product of reaction 3b, which is attached to an Mo atom at the sulfur vacancy site and indicated by a circle in Figure 5, still retains the H−H bond character. According to ref 34, the Kubas interaction energy is in the range of 0.2−0.4 eV and thus in agreement with the reaction energy difference of 0.37 eV between the transition and final states of reactions 3a and 3b.

The Kubas interaction also reduces the reaction barrier and degree of endothermicity considerably. Nevertheless, reactions 3a and 3b are not competitive in comparison with the strongly exothermic reaction 1 with $E_R = -3.09$ eV in thermodynamic equilibrium.

DOI: 10.1021/acsnano.7b04162
ACS Nano 2017, 11, 9989−9996

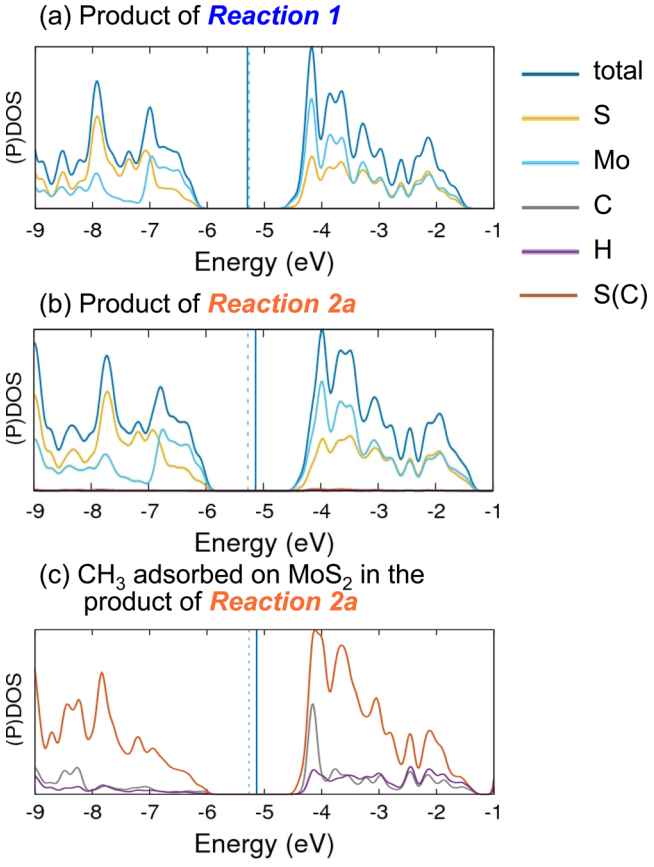

Figure 4. Electronic structure of products of the vacancy healing process shown in Figure 3. Total density of states (DOS) and partial densities of states (PDOS) of the products of reactions (a) 1 and (b) 2a. (c) PDOS of the CH_3 molecule bonded to a sulfur atom in an MoS_2 monolayer. The PDOS of the sulfur atom connected to C in CH_3, S(C), is shown by the brown line. All DOS and PDOS functions have been convoluted by a Gaussian with a full-width at half-maximum of 0.1 eV. The position of the Fermi level is shown by solid blue lines in defective lattices and by dotted blue lines in the corresponding pristine lattices.

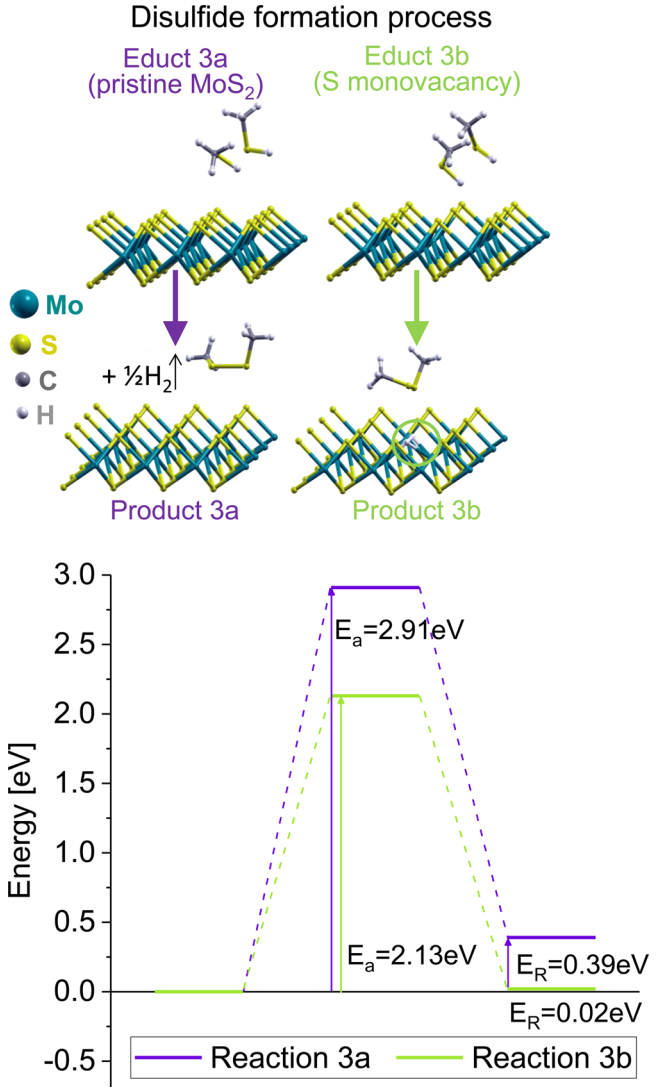

Figure 5. Reaction scheme of the disulfide formation process involving exposure of an MoS_2 monolayer to two CH_3SH molecules. E_R denotes the reaction energy and E_a the activation barrier. Reaction 3a, shown in dark purple, occurs on pristine MoS_2. Reaction 3b, shown in light green, occurs on a sulfur-deficient MoS_2 substrate.

The PDOS functions characterizing the products of reactions 3a and 3b, visualized in Figure 5, are shown in Figure 6. The product of reaction 3b still contains a defect state in the gap region, indicating that the chemisorbed H_2 molecule is incapable of electronically repairing the effect of the sulfur vacancy. This is seen in the PDOS of the Mo atoms of the Kubas complex surrounding the vacancy defect in Figure 6c. The product of reaction 3a, on the other hand, shows no indication of a defect state, since the vacancy-free MoS_2 monolayer is not affected much by the physisorbed disulfide, as seen in the PDOS of Figure 6a.

We can thus conclude that the disulfide formation reaction 3a, suggested in ref 30, is endothermic. The alternative reaction 3b on a sulfur-deficient MoS_2 substrate displays a lower activation barrier and an end-product stabilized by the Kubas interaction, but is still weakly endothermic and thus unlikely. In the following, we propose an alternative pathway toward disulfide formation.

Adatom Repair. The postulated alternative reaction requires extra sulfur atoms adsorbed on the MoS_2 surface, which act as nucleation sites for the disulfide formation. The reaction leading to the formation of disulfide R−SS−R in the presence of sulfur adatoms consists of two steps, described by reactions 4a and 4b, as well as the alternative reaction 4c following reaction 4a, as shown in Figure 7.

In reaction 4a, a CH_3SH molecule interacts with the reactive sulfur adatom to methylhydrodisulfide (CH_3SSH), releasing −0.86 eV due to the formation of a stable disulfide bond. The estimated activation barrier for this reaction is close to 1 eV, which is considerably lower than the values for the corresponding reactions 3a and 3b in absence of an extra sulfur adatom.

Electronic structure changes during the adatom healing process are displayed in Figure 8. The DOS of the product of reaction 4a, shown in Figure 8b, shows no defect-related states in the band gap, indicating chemical and electronic repair of the sulfur adatom defect that is seen in Figure 8a.

In the subsequent reaction 4b, shown in Figure 7, a second CH_3SH molecule interacts with the methylhydrodisulfide CH_3SSH, leading to the exchange of the hydrogen atom with a methyl group and formation of hydrogen sulfide (H_2S) as a side product. This reaction is mildly exothermic, with an overall

DOI: 10.1021/acsnano.7b04162
ACS Nano 2017, 11, 9989−9996

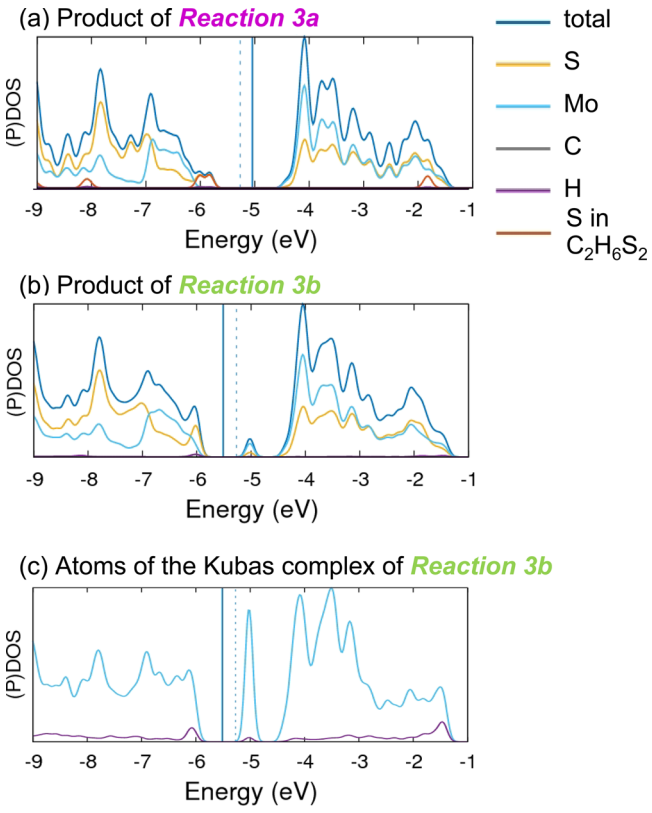

Figure 6. Electronic structure of products of the disulfide formation process shown in Figure 5. Total density of states (DOS) and partial densities of states (PDOS) of the products of reactions (a) 3a and (b) 3b. (c) PDOS of the 3 Mo atoms and the H_2 molecule attached to the vacancy that form the Kubas complex in the product of reaction 3b. All DOS and PDOS functions have been convoluted by a Gaussian with a full-width at half-maximum of 0.1 eV. The position of the Fermi level is shown by solid blue lines in defective lattices and by dotted blue lines in the corresponding pristine lattices.

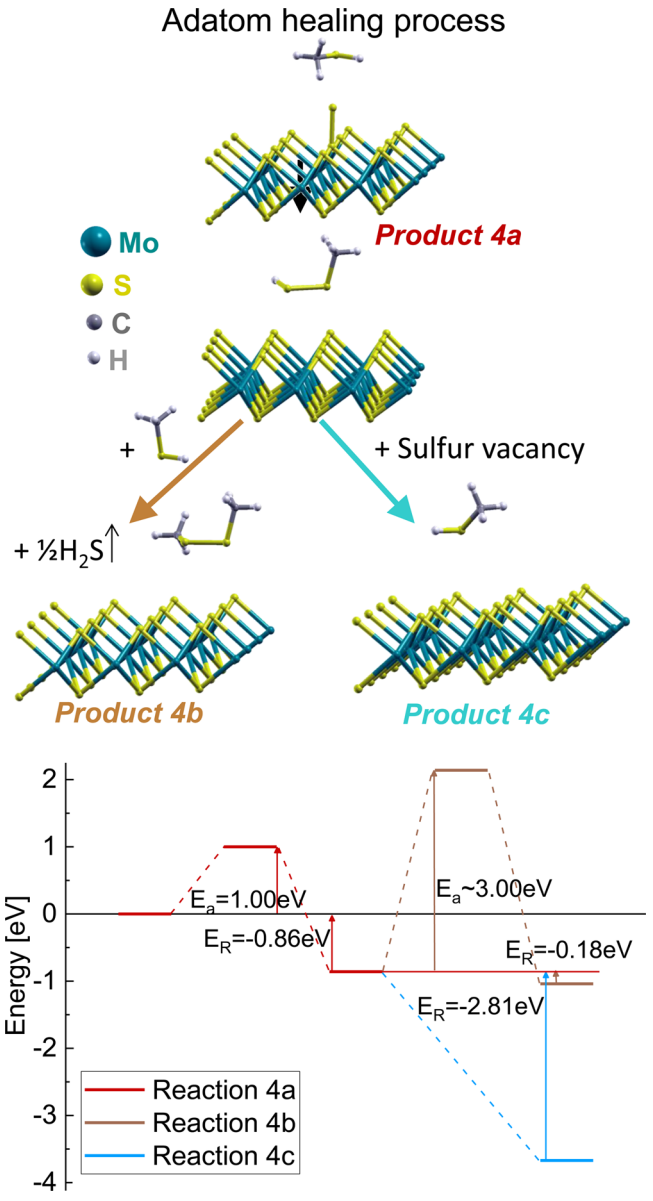

Figure 7. Reaction scheme of the adatom healing process that starts with reaction 4a and leads to disulfide formation in the presence of extra sulfur atoms on MoS_2, shown in dark red. Subsequent ligand exchange reaction 4b is shown in brown. Alternative subsequent vacancy repair reaction 4c is shown in light blue. E_R denotes the reaction energy and E_a the activation barrier.

reaction energy of −0.18 eV. Even though the combined reaction 4a and 4b for the formation of CH_3SSCH_3 is strongly exothermic with a net energy gain of −1.05 eV, the activation barrier for the ligand exchange in reaction 4b is prohibitively high with $E_a \approx +3$ eV, which essentially suppresses the formation of CH_3SSCH_3 following reaction 4a.

Therefore, we investigated reaction 4c as an alternative follow-up process to reaction 4a. In reaction 4c, the CH_3SSH molecule interacts with a nearby sulfur vacancy defect. This reaction is similar to the vacancy healing reaction 1 and consequently is strongly exothermic with a reaction energy of −2.81 eV. Reaction 4c is barrier-free and thus occurs spontaneously. As seen in Figure 8c, describing the product of reaction 4c, the defect-related state above E_F has been removed from the DOS. This means that following the adatom repair and disulfide formation, reaction 4a, reaction 4c will take place in case that sulfur vacancies are also present. The two reactions will thus heal both vacancy and adatom defects.

Our above considerations offer an attractive explanation why disulfide formation was observed in ref 30, but not in refs 21, 22, 28, and 29. Initially, reactions 1 and 4a plus 4c have taken place in all samples that contained vacancies. Vacancy healing as the primary outcome of reactions reported in refs 21, 22, 28, and 29 could likely be achieved due to an abundance of vacancies in the samples used. We may speculate that the MoS_2 sample of ref 30 contained more sulfur adatoms than sulfur vacancies. In that case, all vacancy defects could be repaired, but some adatom defects were left unrepaired in the sample of ref 30. At this point, lack of vacancy defects would block reactions 1 and 4c. The only viable reaction was 4a, which repaired adatom defects, leaving a pristine MoS_2 surface behind with disulfide as a byproduct. This speculative assumption is also consistent with the observation that the electronic structure of MoS_2 has remained unaffected by the reaction leading to the formation of disulfide.[30]

CONCLUSIONS

We studied three different reaction paths of thiols, represented by methanethiol (CH_3SH), with a defective 2D MoS_2 monolayer. We showed that the repair of sulfur monovacancies

DOI: 10.1021/acsnano.7b04162
ACS Nano 2017, 11, 9989−9996

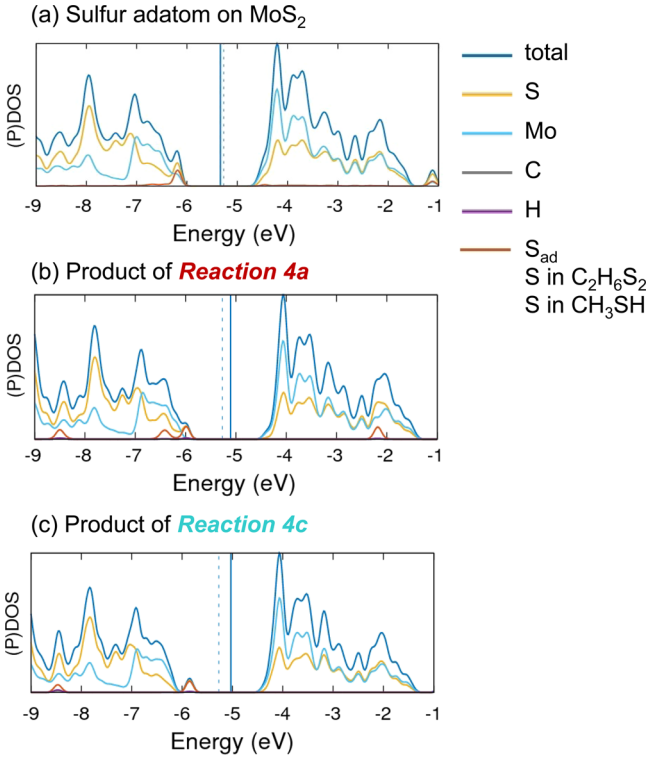

Figure 8. Electronic structure of products of the adatom healing process shown in Figure 7. Total density of states (DOS) and partial densities of states (PDOS) of (a) MoS_2 with a sulfur adatom (without CH_3SH), (b) product of reaction 4a, and (c) product of reaction 4c. All DOS and PDOS functions have been convoluted by a Gaussian with a full-width at half-maximum of 0.1 eV. The position of the Fermi level is shown by solid blue lines in defective lattices and by dotted blue lines in the corresponding pristine lattices.

by adsorbed CH_3SH is an exothermic reaction releasing up to 3 eV. In another possible reaction between CH_3SH and MoS_2, leading to the formation of disulfide, we found that the presence of sulfur vacancies lowers the reaction barrier due to the Kubas interaction at the defect site. The corresponding reaction involving MoS_2 with sulfur adatoms instead of vacancies, on the other hand, leads to disulfide formation and releases about 0.9 eV. In the presence of sulfur vacancies, the formed disulfides will immediately reduce to thiols while simultaneously healing the vacancy defect. We can therefore conclude that, regardless of interim disulfide formation, thiols always lead to a chemical repair of available sulfur vacancies by filling-in the missing sulfur atoms and consequently eliminating vacancy-related defect states in the gap.

THEORETICAL METHODS

To obtain insight into the reaction processes, we performed DFT calculations using the SIESTA code.[35] We used *ab initio* Troullier–Martins pseudopotentials[38] and the PBE exchange–correlation functional[36] throughout the study. Except for sulfur, all pseudopotentials used were obtained from the online resource in ref 39. The pseudopotential of sulfur has been generated without core corrections using the ATM code in the SIESTA suite and the parameters listed in ref 39. All pseudopotentials were tested against atomic all-electron calculations. We used a double-ζ basis set including polarization orbitals (DZP) to represent atoms in crystal lattices, 140 Ry as the mesh cutoff energy for the Fourier transform of the charge density, and 0 K for the electronic temperature. We used periodic boundary conditions with large supercells spanned by the lattice vectors $\vec{a}_1$ = (12.84, 0.00, 0.00) Å, $\vec{a}_2$ = (6.42, 11.12, 0.00) Å, $\vec{a}_3$ = (0.00, 0.00, 22.23) Å to represent pristine and defective 2D MoS_2 lattices. The unit cells of defect-free MoS_2 contained 16 molybdenum and 32 sulfur atoms and were separated by a vacuum region of ≈15 Å normal to the layers. The Brillouin zone was sampled by a 4 × 4 × 1 *k*-point grid[37] and its equivalent in larger supercells.

The above input parameters were found to guarantee convergence. In particular, we found that using the larger triple-ζ polarized (TZP) instead of the DZP basis and increasing the mesh cutoff energy affected our total energy differences by typically less than 0.01 eV. We furthermore validated the *ab initio* pseudopotential approach used in the SIESTA code by comparing to results of the all-electron SCM-Band code[41] and found that energy differences obtained using the two approaches differed typically by less than 0.3 eV.

All geometries have been optimized using the conjugate gradient method,[40] until none of the residual Hellmann–Feynman forces exceeded 10^{-2} eV/Å. In addition to the default density matrix convergence, we also demanded that the total energy should reach the tolerance of $\lesssim 10^{-4}$ eV. To eliminate possible artifacts associated with local minima, we verified initial and final state geometries by performing canonical molecular dynamics (MD) simulations using an NVT-Nosé thermostat with T = 273.15 K and 1 fs time steps.

Due to the complexity of the reaction energy hypersurface and the large number of relevant degrees of freedom, approaches such as the nudged elastic band, which are commonly used to determine the reaction path including transition states, turned out to be extremely demanding on computer resources. We focused on transition states only and initiated our search by running canonical MD simulations starting from a set of educated guesses for the geometry. Following the atomic trajectories, we could identify a saddle point in the energy hypersurface, where all forces acting on atoms vanished, and postulated this point in configurational space as a transition state. To confirm this postulate, we ran MD simulations starting at a slightly altered geometry of the postulated transition state. We concluded that the postulated transition state is indeed the real transition state once all trajectories reached either the initial (educt) or the final (product) state. The activation barrier was determined by the energy difference between the initial and the transition state.

AUTHOR INFORMATION

Corresponding Author

*E-mail: tomanek@pa.msu.edu.

ORCID

Anja Förster: 0000-0002-2203-8662

David Tománek: 0000-0003-1131-4788

Notes

The authors declare no competing financial interest.

ACKNOWLEDGMENTS

We thank Jie Guan and Dan Liu for useful discussions and Garrett B. King for carefully checking the bibliography. This study was supported by the NSF/AFOSR EFRI 2-DARE grant number #EFMA-1433459. Computational resources have been provided by the Michigan State University High Performance Computing Center and the Center of Information Services and High Performance Computing (ZIH) at TU Dresden. A.F., S.G., and G.S. acknowledge funding from the Center for Advancing Electronics Dresden (cfaed). A.F. acknowledges the hospitality of Michigan State University and the cfaed Inspire Grant. S.G. acknowledges funding from the Initiative and Networking Funds of the President of the Helmholtz Association *via* the W3 Programme. G.S. also acknowledges support from NUST "MISis" (No. K3-2017-064).

DOI: 10.1021/acsnano.7b04162
ACS Nano 2017, 11, 9989–9996

REFERENCES

(1) Li, H.; Yin, Z.; He, Q.; Li, H.; Huang, X.; Lu, G.; Fam, D. W. H.; Tok, A. I. Y.; Zhang, Q.; Zhang, H. Fabrication of Single- and Multilayer Mos_2 Film-Based Field-Effect Transistors for Sensing NO at Room Temperature. *Small* **2012**, *8*, 63−67.

(2) Castellanos-Gomez, A.; van Leeuwen, R.; Buscema, M.; van der Zant, H. S.; Steele, G. A.; Venstra, W. J. Single-Layer MoS_2 Mechanical Resonators. *Adv. Mater.* **2013**, *25*, 6719−6723.

(3) Chang, H.-Y.; Yang, S.; Lee, J.; Tao, L.; Hwang, W.-S.; Jena, D.; Lu, N.; Akinwande, D. High-Performance, Highly Bendable MoS_2 Transistors with High-K Dielectrics for Flexible Low-Power Systems. *ACS Nano* **2013**, *7*, 5446−5452.

(4) Ellis, J. K.; Lucero, M. J.; Scuseria, G. E. The Indirect to Direct Band Gap Transition in Multilayered MoS_2 as Predicted by Screened Hybrid Density Functional Theory. *Appl. Phys. Lett.* **2011**, *99*, 261908.

(5) Splendiani, A.; Sun, L.; Zhang, Y.; Li, T.; Kim, J.; Chim, C.-Y.; Galli, G.; Wang, F. Emerging Photoluminescence in Monolayer MoS_2. *Nano Lett.* **2010**, *10*, 1271−1275.

(6) Pachauri, V.; Kern, K.; Balasubramanian, K. Chemically Exfoliated Large-Area Two-Dimensional Flakes of Molybdenum Disulfide for Device Applications. *APL Mater.* **2013**, *1*, 032102.

(7) Li, H.; Wu, J.; Yin, Z.; Zhang, H. Preparation and Applications of Mechanically Exfoliated Single-Layer and Multilayer MoS_2 and WSe_2 Nanosheets. *Acc. Chem. Res.* **2014**, *47*, 1067−1075.

(8) Varrla, E.; Backes, C.; Paton, K. R.; Harvey, A.; Gholamvand, Z.; McCauley, J.; Coleman, J. N. Large-Scale Production of Size-Controlled MoS_2 Nanosheets by Shear Exfoliation. *Chem. Mater.* **2015**, *27*, 1129−1139.

(9) Samassekou, H.; Alkabsh, A.; Wasala, M.; Eaton, M.; Walber, A.; Walker, A.; Pitkänen, O.; Kordas, K.; Talapatra, S.; Jayasekera, T.; Mazumdar, D. Viable Route towards Large-Area 2D MoS_2 Using Magnetron Sputtering. *2D Mater.* **2017**, *4*, 021002.

(10) Kastl, C.; Chen, C. T.; Kuykendall, T.; Shevitski, B.; Darlington, T. P.; Borys, N. J.; Krayev, A.; Schuck, P. J.; Aloni, S.; Schwartzberg, A. M. The Important Role of Water in Growth of Monolayer Transition Metal Dichalcogenides. *2D Mater.* **2017**, *4*, 021024.

(11) Keller, B. D.; Bertuch, A.; Provine, J.; Sundaram, G.; Ferralis, N.; Grossman, J. C. Process Control of Atomic Layer Deposition Molybdenum Oxide Nucleation and Sulfidation to Large-Area MoS_2 Monolayers. *Chem. Mater.* **2017**, *29*, 2024−2032.

(12) Browning, R.; Padigi, P.; Solanki, R.; Tweet, D. J.; Schuele, P.; Evans, D. Atomic Layer Deposition of MoS_2 Thin Films. *Mater. Res. Express* **2015**, *2*, 035006.

(13) Kwon, D. H.; Jin, Z.; Shin, S.; Lee, W.-S.; Min, Y.-S. A Comprehensive Study on Atomic Layer Deposition of Molybdenum Sulfide for Electrochemical Hydrogen Evolution. *Nanoscale* **2016**, *8*, 7180−7188.

(14) Vancsó, P.; Magda, G. Z.; Petö, J.; Noh, J.-Y.; Kim, Y.-S.; Hwang, C.; Biró, L. P.; Tapasztó, L. The Intrinsic Defect Structure of Exfoliated MoS_2 Single Layers Revealed by Scanning Tunneling Microscopy. *Sci. Rep.* **2016**, 610.1038/srep29726.

(15) Addou, R.; McDonnell, S.; Barrera, D.; Guo, Z.; Azcatl, A.; Wang, J.; Zhu, H.; Hinkle, C. L.; Quevedo-Lopez, M.; Alshareef, H. N. Impurities and Electronic Property Variations of Natural MoS_2 Crystal Surfaces. *ACS Nano* **2015**, *9*, 9124−9133.

(16) Liu, K.-K.; Zhang, W.; Lee, Y.-H.; Lin, Y.-C.; Chang, M.-T.; Su, C.-Y.; Chang, C.-S.; Li, H.; Shi, Y.; Zhang, H. Growth of Large-Area and Highly Crystalline MoS_2 Thin Layers on Insulating Substrates. *Nano Lett.* **2012**, *12*, 1538−1544.

(17) Lee, Y.-H.; Zhang, X.-Q.; Zhang, W.; Chang, M.-T.; Lin, C.-T.; Chang, K.-D.; Yu, Y.-C.; Wang, J. T.-W.; Chang, C.-S.; Li, L.-J. Synthesis of Large-Area MoS_2 Atomic Layers with Chemical Vapor Deposition. *Adv. Mater.* **2012**, *24*, 2320−2325.

(18) Zhan, Y.; Liu, Z.; Najmaei, S.; Ajayan, P. M.; Lou, J. Large-Area Vapor-Phase Growth and Characterization of MoS_2 Atomic Layers on a SiO_2 Substrate. *Small* **2012**, *8*, 966−971.

(19) Hong, J.; Hu, Z.; Probert, M.; Li, K.; Lv, D.; Yang, X.; Gu, L.; Mao, N.; Feng, Q.; Xie, L.; Zhang, J.; Wu, D.; Zhang, Z.; Jin, C.; Ji, W.; Zhang, X.; Yuan, J.; Zhang, Z. Exploring Atomic Defects in Molybdenum Disulphide Monolayers. *Nat. Commun.* **2015**, *6*, 6293.

(20) Amani, M.; Lien, D.-H.; Kiriya, D.; Xiao, J.; Azcatl, A.; Noh, J.; Madhvapathy, S. R.; Addou, R.; KC, S.; Dubey, M.; Cho, K.; Wallace, R. M.; Lee, S.-C.; He, J.-H.; Ager, J. W.; Zhang, X.; Yablonovitch, E.; Javey, A. Near-Unity Photoluminescence Quantum Yield in MoS_2. *Science* **2015**, *350*, 1065−1068.

(21) Yu, Z.; Pan, Y.; Shen, Y.; Wang, Z.; Ong, Z.-Y.; Xu, T.; Xin, R.; Pan, L.; Wang, B.; Sun, L.; Wang, J.; Zhang, G.; Zhang, Y. W.; Shi, Y.; Wang, X. Towards intrinsic charge transport in monolayer molybdenum disulfide by defect and interface engineering. *Nat. Commun.* **2014**, *5*, 5290.

(22) Makarova, M.; Okawa, Y.; Aono, M. Selective Adsorption of Thiol Molecules at Sulfur Vacancies on MoS_2 (0001), Followed by Vacancy Repair *via* S-C Dissociation. *J. Phys. Chem. C* **2012**, *116*, 22411−22416.

(23) Surrente, A.; Dumcenco, D.; Yang, Z.; Kuc, A.; Jing, Y.; Heine, T.; Kung, Y.-C.; Maude, D. K.; Kis, A.; Plochocka, P. Defect Healing and Charge Transfer-Mediated Valley Polarization in $MoS_2/MoSe_2/MoS_2$ Trilayer van der Waals Heterostructures. *Nano Lett.* **2017**, *17*, 4130−4136.

(24) Noh, J.-Y.; Kim, H.; Kim, Y.-S. Stability and Electronic Structures of Native Defects in Single-Layer MoS_2. *Phys. Rev. B: Condens. Matter Mater. Phys.* **2014**, *89*, 205417.

(25) Santosh, K.; Longo, R. C.; Addou, R.; Wallace, R. M.; Cho, K. Impact of Intrinsic Atomic Defects on the Electronic Structure of MoS_2 Monolayers. *Nanotechnology* **2014**, *25*, 375703.

(26) Ghorbani-Asl, M.; Enyashin, A. N.; Kuc, A.; Seifert, G.; Heine, T. Defect-Induced Conductivity Anisotropy in MoS_2 Monolayers. *Phys. Rev. B: Condens. Matter Mater. Phys.* **2013**, *88*, 245440.

(27) Sim, D. M.; Kim, M.; Yim, S.; Choi, M.-J.; Choi, J.; Yoo, S.; Jung, Y. S. Controlled Doping of Vacancy-Containing Few-Layer MoS_2 via Highly Stable Thiol-Based Molecular Chemisorption. *ACS Nano* **2015**, *9*, 12115−12123.

(28) Peterson, S. L.; Schulz, K. H. Ethanethiol Decomposition Pathways on MoS_2 (0001). *Langmuir* **1996**, *12*, 941−945.

(29) Wiegenstein, C. G.; Schulz, K. H. Methanethiol Adsorption on Defective MoS_2 (0001). *J. Phys. Chem. B* **1999**, *103*, 6913−6918.

(30) Chen, X.; Berner, N. C.; Backes, C.; Duesberg, G. S.; McDonald, A. R. Functionalization of Two-Dimensional MoS_2: On the Reaction Between MoS_2 and Organic Thiols. *Angew. Chem., Int. Ed.* **2016**, *55*, 5803−5808.

(31) Benziger, J. B.; Preston, R. E. Organosulfur Chemistry on Tungsten (211) Surfaces. 1. A Comparison of Methanethiol and Methanol. *J. Phys. Chem.* **1985**, *89*, 5002−5010.

(32) Kubas, G. J. Five-Co-Ordinate Molybdenum and Tungsten Complexes, $[M(CO)_3(PCy_3)_2]$, which Reversibly Add Dinitrogen, Dihydrogen, and Other Small Molecules. *J. Chem. Soc., Chem. Commun.* **1980**, 61−62.

(33) Gordon, J. C.; Kubas, G. J. Perspectives on How Nature Employs the Principles of Organometallic Chemistry in Dihydrogen Activation in Hydrogenases. *Organometallics* **2010**, *29*, 4682.

(34) Skipper, C. V. J.; Hamaed, A.; Antonelli, D. M.; Kaltsoyannis, N. The Kubas Interaction in M(II) (M = Ti, V, Cr) Hydrazine-Based Hydrogen Storage Materials: A DFT Study. *Dalton Trans.* **2012**, *41*, 8515−8523.

(35) Soler, J. M.; Artacho, E.; Gale, J. D.; García, A.; Junquera, J.; Ordejón, P.; Sánchez-Portal, D. The SIESTA Method for *Ab Initio* Order-N Materials Simulation. *J. Phys.: Condens. Matter* **2002**, *14*, 2745.

(36) Perdew, J. P.; Burke, K.; Ernzerhof, M. Generalized Gradient Approximation Made Simple. *Phys. Rev. Lett.* **1996**, *77*, 3865.

(37) Monkhorst, H. J.; Pack, J. D. Special Points for Brillouin-Zone Integrations. *Phys. Rev. B* **1976**, *13*, 5188.

(38) Troullier, N.; Martins, J. L. Efficient Pseudopotentials for Plane-Wave Calculations. *Phys. Rev. B: Condens. Matter Mater. Phys.* **1991**, *43*, 1993−2006.

DOI: 10.1021/acsnano.7b04162
ACS Nano 2017, 11, 9989−9996

(39) http://departments.icmab.es/leem/siesta/Databases/Pseudopotentials/periodictable-gga-abinit.html, accessed on August 1, 2016.
(40) Hestenes, M. R.; Stiefel, E. Methods of Conjugate Gradients for Solving Linear Systems. *J. Res. Natl. Bur. Stand.* **1952**, *49*, 409−436.
(41) *BAND2017, SCM*, Theoretical Chemistry; Vrije Universiteit: Amsterdam, The Netherlands, http://scm.com, accessed on June 22, 2016.

DOI: 10.1021/acsnano.7b04162
ACS Nano 2017, 11, 9989−9996